Evaluation of *in vitro* and *in vivo* toxicity of pristine molybdenum disulphide nanosheets in Swiss albino mice

Umakant Yadav [a], *Vimal Singh* [a], *Himanshu Mishra*[b], *Preeti S. Saxena*[a*], *Anchal Srivastava*[b*]

[a]Department of Zoology, Institute of Science, Banaras Hindu University, Varanasi-221005, India.

[b]Department of Physics, Institute of Science, Banaras Hindu University, Varanasi-221005, India.

[*]**Corresponding authors**

Email: pssaxena@rediffmail.com (Dr. Preeti S. Saxena)

Keywords: MoS_2, oxidative stress, haematology, histopathology, toxicity, antioxidants.

Abstract:

The Molybdenum disulfide nanosheets (MoS_2-NSs) thin films has received increasing attention recently due to their versatile multi functionality including catalytic properties, photoluminescence and flexibility, which suggests their future, uses for biomedical applications. However, there are no studies in detail related with biocompatibility of MoS_2 thin sheets. Here, weevaluated the dose-dependent effects of MoS_2-NSs on cell viability (MTT assay) and release of lactate dehydrogenase (LDH) into culture media using MG-63 cells, as well as haemolysis, hematological, serum biochemical, antioxidants and histopathological parameters in *Swiss albino* mice. The MoS_2-NSs was synthesized *via* facile hydrothermal method and characterized using XRD, Raman, SEM, TEM and HRTEM. The *in vitro* study results suggest that at lower concentration MoS_2-NSs does not causes any toxicity. The lethal dose (LD50) was evaluated by intraperitoneal administration with different concentrations and estimated as ~1.0 mg kg^{-1}. The higher dose (1.5 mg kg^{-1}) of MoS_2-NSs showed significant alteration in hematological markers and serum biochemical enzymes, as compared to control. Lipid peroxidation also shows significant alteration with respect to the control. Histopathological, hematological and biochemical examination, revealed no remarkable changes at lower concentration (less than 1.0 mg kg^{-1}), however, higher concentration (1.5 mg kg^{-1}) causes significant histopathological, antioxidants and biochemical alterations in tissues and serum, respectively. The results suggest that the lower concentration of MoS_2-NSs can be used in future biomedical applications.

1. Introduction

In recent years, transition metal dichalcogenides (TMDs), a class of 2D nanomaterials, have spurred different areas of engineering, material science, and chemistry due to their unique physiochemical properties[1,2]. TMDs such as MoS_2, WS_2, $MoSe_2$ and WSe_2 are hexagonal layers and can be symbolized with the general formula MX_2, where M represents a transition metal element from (Mo and W) and X represents a chalcogen (S, Se, Te). TMDs have layered structures arranged in the X-M-X conformation with in-plane covalent bonding and weak Van der Waal's forces of attraction between layers[3,4].Molybdenum disulfide (MoS_2), a member of TMDs family, has been studied extensively analogous to grapheme [5–7].

In recent years, TMDs have attracted attention as a new non-viral gene delivery vehicle and in cancer therapy[8–10].Reports are available that appropriate surface modification of molybdenum disulfide nanosheets (MoS_2-NSs) with PEG and PEI served as a unique 2D nanocarrier for efficient siRNA delivery for PLK1 gene silencing[11], sensing applications[12], bone tissue engineering[13]and bioimaging [14]. The electrochemical sensing behavior of single-layer MoS_2-NSs has been described, for glucose sensing as well as for the specific detection of dopamine[15,16]. In addition, MoS_2-NSs have been also reported as template for hybridization of DNA strands and immunoglobulin's for sensing of dopamine and ascorbic acid[17,18].MoS_2 act as guided missile for targeting of lung cancer. High mechanical strength of MoS_2-NSs serves as an efficient reinforcing material for load bearing application and in tissue engineering[19].

Despite of its ($MoS_{2)}$ countless applications, there is no report available on MoS_2-NSs *in vivo* toxicity in animal models. Therefore, as a successful candidate for *in vivo* applications in bio- and nanomedicine, *in vitro* and *in vivo* study of MoS_2-NSs is highly desirable.

Keeping above points in view, here we have evaluated *in vitro* and *in vivo* toxicity study of MoS_2-NSs using MG-63 cells and in *Swiss albino* mice in terms of hematological, serum biochemical analysis, lipid peroxidation assay, antioxidants enzymes analysis and histopathological examinations.

2. Experimental Details

2.1 Chemicals

Sodium molybdatedehydrate ($Na_2MoO_4.2H_2O$), hydrochloric acid (HCl), ethanol, hematoxylin–eosin stain and glacial acetic acid were purchased from Sigma Aldrich, New Delhi, India. Xylene, ethyl alcohol, paraffin wax, and microscope slides were obtained from Thermo-Fisher Scientific Pvt. Ltd. India. Serum biochemical enzymes (AST, ALT, and ALP) kits were procured from Beacon Pvt. Ltd. India. Antioxidant assay reagents were purchased from Merck Pvt. Ltd. India. All the chemicals and reagents were of analytical grade and used without any further purification.

2.2 Preparation of MoS_2-NSs

MoS_2-NSs have been synthesized using facile and eco-friendly hydrothermal method with some modifications[20]. In a typical synthesis route, 0.25g sodium molybdate and 0.5g of L-Cysteine were dissolved in 25 ml and 50 ml di-ionized (DI) water separately. These two solutions were stirred for 10 minutes at 40°C for complete dissolution of the precursors. Both the solutions were poured in a single beaker and mixed under constant stirring. The pH of the solution was maintained at ~5 using 0.1M HCl. Finally, the solution was transferred to a 100 ml capacity stainless steel lined Teflon autoclave. The Teflon autoclave was put in an oven and

temperature of the oven was maintained at 230°C for 40 hour. After the completion of the reaction the black color sample has been taken out, which was washed with ethanol and distilled water thrice. The washed sample was dried for 12 hours at 60°C in open atmosphere.

2.3 Cell Culture

The MG-63 cells (human osteoblast) were procured from National Centre for Cell Sciences (NCCS) Pune, India and cultured in standard Dulbecco's Modified Eagle Medium(DMEM), supplemented with 10% fetal bovine serum (FBS), and1% penicillin/streptomycin antibiotics under controlled atmospheric conditions(37°C temperature and 5% CO_2). The old culture medium was replaced every 2−3 days and cells were sub-cultured after 3−4 days when cell confluency reached about 80-85%.

2.4 Cell Viability

MTT (3-dimethylthiazol-2, 5-diphenyltetrazolium bromide) assay was perform to evaluate the cell viability after 24 h of cell seeding in the presence and absence ofMoS_2-NSs suspensions. Typically, MG-63 cells were seeded in 96 well culture plates with a density 1×10^5cells/well and incubated for 24 h for initial attachment. After 24 h, the media was replaced with medium having variable concentrations (2, 5, 10, 20, 40, 80, 100, 200,400 and 800 μgml^{-1}) of nanocomposite suspensions (Stock concentration 1.0 $mgml^{-1}$) and incubated for 24h. After incubation cells were washed twice with PBS and incubated again with media containing 0.5 $mgml^{-1}$MTTfor 4 h at 37 °C under 5% CO_2 to form formazan crystals. Finally, MTT containing medium was removed and 100µL of dimethylsulfoxide (DMSO) was added followed by incubation on a rocking shaker for 20 min at 37 °C to dissolute the formazan crystals. After

complete dissolution, absorbance of supernatant was recorded at 540nm using a microplate reader (BioTek, USA). The wells without MoS_2-NSssuspensions were used as controls. The values were represented as the mean ± standard deviation (n= 3). Cell viability was calculated using the formula.

$$Cell\ viability\ (\%) = \frac{[Abs_{test}]}{[Abs_{control}]} \times 100$$

2.5 Lactate Dehydrogenase (LDH) release

Lactate dehydrogenase (LDH) assay was performed to evaluate the biocompatibility of MoS_2-NSs.MG-63 cells with a density 1×10^5cells/well were seeded in a 96-well plate and incubated with different concentrations(2, 5, 10, 20, 40, 80, 100, 200,400 and 800 μgml^{-1}) of MoS_2-NSs suspensions at37 °C under 5% CO_2 for 24 hours. Standard LDH solution (1 ml) was added to the supernatant and the absorbance of the supernatant was recorded at 490 nm to analyze the level of LDH release. The wells without MoS_2-NSs suspensions were used as negative controls and cells treated with Triton X-100 taken as positive control.

$$LDH\ release\ (\%) = (LDH_{sample} - LDH_{negative})/(LDH_{positive} - LDH_{negative}) \times 100$$

2.6 Haemolytic analysis

Haemolytic activities of MoS_2-NSs were evaluated by detecting the haemoglobin release from red blood cells (RBCs). Blood was collected in polypropylene tubes with anti-coagulant EDTA from healthy male *swiss albino* mice. The RBC was isolated from blood by centrifugation (3000 rpm at 4 °C for 10 min) and washed five times with PBS solution (pH 7.4). Then, the RBC was diluted ten times with PBS. Furthermore, the RBC suspension was added to theMoS_2-NSssuspension in a volume ratio of 1:4 to give a final concentration of 25-800 μgml^{-1}. PBS solution and Triton X-100were used as the negative (0% lysis) and positive (100% lysis)

controls, respectively. The RBC suspensions were incubated at37 °C for 45 min. Subsequently, all the suspensions were centrifuged at 3000 rpm at room temperature for 10 min, and the absorbance at 541 nm was recorded microplate reader (BioTek).The percentage haemolysis was expressed by the formula given below.

$$Percentage\ hemolysis\ (\%) = (A_{sample} - A_{negative})/(A_{positive} - A_{negative}) \times 100$$

where, A_{sample}, $A_{negative}$, and $A_{positive}$represent the absorbanceof the samples and negative and positive controls, respectively.

2.7 Animal Maintenance

All experiments with animal were carried out in compliance with the institutional ethics committee regulations and guidelines on animal welfare (Animal Care and Use Program Guidelines of IMS, BHU) and approved by Government of India.

Male *Swiss Albino* mice (~32 g), 3-5 weeks old, were procured from Institute of Medical Sciences, Banaras Hindu University, India. Mice were kept in cages (five mice per cage) and maintained under 12:12 hour light and dark photo period. Mice were fed with controlled *ad libitum* and water.

2.8 Lethal dose (LD50) estimation

For toxicological evaluation of MoS_2-NSs, LD50 was evaluated using Irwin's test method[21]. After acclimatization, twenty five mice were randomly divided into five groups, and each group contains five mice. One group was selected as control (0.9% saline), and rest four groups were selected as the experimental groups (0.5, 1.0 and 1.5 $mgkg^{-1}$). After single dose administration of MoS_2-NSs, animals were observed for behavior and clinical signs of lethargy for 8 days.

2.9Study design

The homogeneous solution of MoS_2-NSs was prepared in sterile 0.9% saline (Misonix, Long Island, NY, USA) using sonication at 40% amplitude with pulse 2 seconds on-off cycle for 30 min. The concentration of the stock solution was 1.0 $mgml^{-1}$. After acclimatization, twenty mice were randomly divided into four groups, each containing five mice. One group was selected as control (0.9% saline), and rest three as the experimental groups. The MoS_2-NSs suspension was administered intraperitoneal to the experimental groups (I, II & III) having concentrations ~0.5 mg kg^{-1}, 1.0 mg kg^{-1} and 1.5 $mgkg^{-1}$, respectively. The time interval between dose administrations was 24 hour, up to 8 days. Body weight of each mouse was recorded before and after dose administration after every two days.

Different vital organs such as (liver, kidney and spleen) were excised aseptically and weighted carefully for organ indices calculations. A portion of each organ (liver, kidney and spleen) were cut off and immediately fixed into Bouin's solution for histopathology. The remaining tissues were stored at −80 ℃ for further biochemical assay.

2.10Hematological and Serum biochemical analysis

The mice were anaesthetized using diethyl ether and decapitated on eight days after six hours from the last dose. The blood was collected for hematological assays. The whole blood (~2.0 ml) was collected in polypropylene tubes with anti-coagulant EDTA (Ethylene diamine tetra acetic acid). Simultaneously, the serum has been separated by centrifugation of clotted blood (~37˚C for 30 min) at 4000 rpm for 10 minute from whole blood maintained at 4˚C. The serum was carried out to measure the level of different enzymes *viz.* alanine aminotransferase (ALT), aspartate aminotransferase (AST) and alkaline phosphatase (ALP) using colorimetric

assay kits procured from Beacon Pvt. Ltd. India. Analysis of blood element *viz.* red blood cell counts (RBCs), hemoglobin (Hb), white blood cells (WBCs), mean corpuscular hemoglobin concentration (MCHC), platelet count (PLT), mean corpuscular hemoglobin (MCH), mean corpuscular volume (MCV) and hematocrit (HCT) were carried out using hematological auto-analyzer (MS-9-3 France).

2.11Preparation of Homogenates

The different organs (liver, kidney and spleen) were excised out on ice-cold physiological saline and cleaned properly. The tissues were used to prepare a 10% w/v homogenate separately in 0.1 M phosphate buffer (pH 7.4) containing 0.1mM EDTA using a motor driven Teflon-pestle homogenizer (Fischer-Scientific), and centrifuged at 12000 rpm for 5 min at 4°C to separate the supernatant. After centrifugation, supernatant was collected and stored at -80 ˚C for further assays. The protein concentration was measured by Bradford method using bovine serum albumin as standard [22].

2.12Lipid peroxidation assay

The level of lipid peroxidation (MDA) in different tissues were measured using thiobarbituric acid (TBA) described by Ohkawa *et. al.*[23].The level of MDA was measured in nmolemg^{-1} protein**.** The supernatant was mixed with 2.8 mM butylated hydroxyl toluene (BHT), 8.1% SDS, 20% Glacial Acetic acid and 0.8% Thiobarbituric acid (TBA) following a boiling at 100 ˚C in water bath for 1 hrs. The reaction was instantaneously transferred into running water and vigorously shaken with n-butanol: pyridine (15:1). The mixture was centrifuged at 1500g for 10 minute and the absorbance spectra of the supernatant have been recorded using UV-Vis spectrophotometer at 534 nm.

2.13Superoxide dismutase assay

A 10% homogenates of different tissues were processed for SOD activity assay as per the mentioned protocol[24].100 µl of the different tissues homogenate were mixed in a 1.4 ml reaction mixture containing 20 mM L-Methionine, 1% (v/v) Triton X-100, 10 mM Hydroxylamine hydrochloride and 50 mM EDTA. After that 80 µl of 50 µM Riboflavin was added and the mixture was illuminated under 20W white light for 10 min. The reaction was stopped by adding freshly prepared Greiss reagent and recorded the absorbance spectra at 543 nm.

2.14Catalase activity assay

10% homogenates of different tissues were processed for the assay in a reaction mixture comprising 0.8 mM H_2O_2, PBS and Potassium dichromate in Glacial Acetic Acid. The reaction was stopped by heating it in a water bath for 10 min and the absorbance spectra has been measured at ~570 nm to monitor the decrement in H_2O_2content. The residual H_2O_2 concentration after depletion by enzyme present in different extract was measured by spectrometer at ~570 nm and depicted as Catalase Activity. The standard curve was calibrated with varying concentrations of 0.2 mM H_2O_2 in PBS[25].

2.15Glutathione peroxidase assay

Different tissue homogenates were handled for protein estimation. 150 µg of protein was mixed in a reaction mixture containing 50 mM phosphate buffer pH 7, 1 mM EDTA, 1 mM sodium azide, 0.5 mM NADPH, 0.2 mM reduced glutathione (GSH) and 1 unit of glutathione reductase. The reaction was put at room temperature for 1 minute to equilibrate. The reaction was started by adding 0.1 mM H_2O_2 and the decrease in the absorbance of reaction mixture was

recorded at ~340 nm for 3 minutes at every 30 seconds interval in the UV-Vis spectrophotometer. The glutathione peroxidase activity was expressed as nanomole of NADPH oxidized/mg protein/ minute according to the procedure reported by Mantha *et al.* [26].

2.16Histopathological Analysis

The organs (liver, kidney and spleen) were surgically excised out from mice under diethyl ether anesthesia. A small piece of the tissue was excised from whole organs and washed with ice-cold normal saline (0.9% NaCl) and 20mM EDTA to remove blood traces. Further, the tissues were cut into small pieces and fixed immediately in Bouin's solution for next 24 h. After fixation, the tissues were transferred to 70% ethyl alcohol and stored until processed. The tissue specimens (liver, kidney, spleen) were processed, embedded in paraffin, sliced into 0.5µm thicknesses, mounted on glass microscope slide and stained with hematoxylin and eosin (H&E) for histological examination under optical microscope. At least 10 slides were selected for histopathological evaluation of each sample.

2.17Apoptotic cells analysis

Apoptotic splenocytes were spotted via Acridine orange (AO) – Ethidium bromide (EtBr) double stain. AO stained both types of cells i.e. apoptotic cells and viable cells emit green fluorescence. Early apoptotic cells exhibits membrane blebbing and chromatin strengthening as bright green spots or fragments while late apoptotic cells indicates orange to red nuclei having compressed or fragmented chromatin. EtBr stained only dead cells and emits red fluorescence when intercalated by DNA. Cells were centrifuged at 1000g for 5 minute to settled and add 100 µl of AO (100 $\mu g ml^{-1}$) and EtBr (100 $\mu g ml^{-1}$) in 1:1 ratio to the cell pellet. After 2–5 minutes a drop of stained cells were taken on a glass slide and mounted with a cover slip and examined

under fluorescence microscope (Leitz MPV3, Wetzlar, Hesse, Germany) centered at ~520 nm emission for a ~440 nm excitation at 920 X magnifications[27].

2.18Statistical Analysis

Statistical analysis was performed using SPSS 16.0 software. All experiments were repeated three independent times and all data were expressed as means ± SEM (standard error mean). One-way analysis of variance (ANOVA) followed by Dunnett's post hoc test with *p*-values less than 0.05 was considered as statistically significant.

3. Results and Discussion

Applications of nanoscale materials have received a tremendous concern in nano-biotechnology due to their unique physiochemical properties. Prolonged exposure of nanomaterials may cause adverse effect on human health and environment. Particularly emerging applications of transition metal chalcogenides with unique optoelectronic and catalytic properties such as MoS_2 for future biomedical applications warrants detail biocompatibility analysis *in vivo*. There is numerous in vitro biocompatibility analyses of surface modified MoS_2-NSs. To the best of our knowledge this is the first report about the *in vivo* toxicity of MoS_2-NSs with *Swiss albino* mice. Our results revealed that MoS_2-NSs (1.5 $mgkg^{-1}$) suppresses the activity of anti-oxidants and causes vital organ injuries.

3.1 Structural/microstructural and morphological characterizations of MoS_2-NSs:

Schematic in figure 1 demonstrate the detail plan for synthesis and *in vivo* toxicity evaluation. Structural/microstructural and morphological characterizations of MoS_2-NSs have been performed using X-ray diffraction (XRD), Raman, scanning electron microscopy

(SEM),and high resolution transmission electron microscopy (HRTEM) **(Figure 2)**. Figure 2(a) shows the XRD pattern of MoS_2-NSs. XRD peaks have been fitted for Gaussian function. All the three peaks have been indexed for the hexagonal phase of MoS_2 with space groups P63/mmc (JCPDS Card no. 37-1492).Plane (00.2) appears at ~13.99° which is slightly smaller than the peak position for bulk MoS_2. Similarly, XRD peak corresponding to the (10.0) appears at ~38.17°, slightly larger than the corresponding value for bulk MoS_2. This confirms that there is an expansion along [001] direction and in-plane compression[28]. Further, synthesized sample is characterized using Raman spectroscopy. A typical Raman spectrum is shown in Figure 2(b), where two peaks E^1_{2g} and A_{1g}pronounces at ~383 cm^{-1} and 409 cm^{-1} is observed. These two peaks correspond to the vibrational mode of first order Raman active center in plane and out of plane phonon vibration of 2H-MoS_2-NSs respectively (Figure 2(c)). The spacing (Δ) between the peak positions E^1_{2g} and $A_{1g}$is found to be ~26 cm^{-1} which confirms that the synthesized MoS_2-NSs are multilayer in nature[29].Figure 2(d) shows the SEM micrograph of MoS_2-NSs. It reveals that the MoS_2-NSs are of few microns in lateral dimensions. TEM micrograph of MoS_2-NSs has been shown in Figure 2(e). TEM image shows that the MoS_2-NSs have agglomerated thin flakes structure. HRTEM image (Figure 2(f)) shows that the MoS_2-NSs are multilayered in nature which is consistent with our Raman results. Inset (Figure 2(f)) shows the Fast Fourier Transform (FFT) pattern and interlayer spacing of MoS_2-NSs. FFT image reveals that the stacking of layers is along c-axis. Interlayer separation is found to be ~0.68 nm, which corresponds to the (00.2) plane of MoS_2-NSs. The interlayer separation corresponding to the (00.2) plane for MoS_2-NSs is found to be slightly larger than the bulk (~0.62 nm), which shows that MoS_2-NSs are swallowed along c-axis[30,31].

3.2 Cell Viability

Cell viability of the MoS_2-NSssuspensions was investigated by MTT assay. The MG-63cells were incubated with different concentration of MoS_2-NSssuspensions (0, 2, 5, 10, 20, 40, 80, 100, 200,400 and 800 μgml^{-1}) for 24 h. As shown in Figure 3a, results reveal that the viability of cells incubated with different concentration of MoS_2-NSssuspensions showed no significant difference between them ($p > 0.05$) on 24 hour up to 40 μgml^{-1}. This shows that the cell viability was not affected by MoS_2-NSs. Meanwhile, cells incubated with higher concentration than 80 $\mu gml^{-1}$of MoS_2NSs suspensions show a significant decrease in cell number Figure 3a. It may be due to lack of proper washing of MoS_2-NSs. Wu *et al.* and Farshid *et al.* reported that MoS_2-NSs have good biocompatibility with human cell lines[32,33].While cells incubated with 400 and 800 $\mu gml^{-1}$of MoS_2-NSssuspension shows significant decreased cell viability. Available reports suggest that toxicity of MoS_2-NSs depends on their synthesis routes[34]. Chang et al. have been reported that the level of toxicity of MoS_2-NSs increases with the increase of exfoliation[34].This is mainly due to the availability of large surface area and more active sites which may leads to the ROS (reactive oxygen species) generation. Studies conducted by Zhang et al. for targeted imaging and photo thermal therapy using RGD-QD-MoS_2NSs against HeLa cells showed no significant toxicity[35].In our synthesis method, we have used sodium molybdate and L-cysteine as starting materials for the synthesis of MoS_2-NSs. In our case, some toxicity appears, it may due to two facts. First, if we consider individual reagents, then hydrolysis of sodium molybdate yields NaOH, H_2O, and a small amount of MoO_3that may be absorbed within the body or eliminated with urine. Further, L-cysteine is a semi essential amino acid and obtained by the hydrolysis of animal materials, so it will also show no toxicity. Second, if we choose MoS_2as an entity to discuss its toxicity, then, as Yin et al. reported, the functionalization ofMoS_2-NSs leads to improved antibacterial property. Our

hydrothermally synthesized MoS_2-NSs is also functionalized that has been already in our earlier work[20,36].Thus, the results of cell viability demonstrate that MG-63cells have good proliferation rate in lower concentration of MoS_2-NSssuspension.

3.3 LDH release

Lactate dehydrogenase (LDH) is a cytoplasmic enzyme that is found in all cells.In the case of mitochondrial and plasma membrane damage, intracellular LDH molecules are released into culture medium. In our study, LDH release profiles were evaluated with respect toMoS_2-NSsconcentration. From the result presented in Figure 3b, it was evident that cell toxicity and LDH release profiles do not show any potential toxicity, showing a low LDH release amount (below 4%) and high cell viability after treatment. The results were in agreement with earlier reports that used PEG-GQDs for toxicity evaluation [37,38].

3.4Haemolysis assay

The hemocompatibility study of any nanomaterial with blood components is a crucial toxicological parameter for the application of nanomaterials for biomedical applications. To address the concern of blood compatibility, a haemolysis assay was also performed against different concentrations ofMoS_2-NSs (25–800 $\mu g ml^{-1}$) for 45 min and the result has been presented in Figure 4. The haemolysis percentages of MoS_2-NSs were also calculated by taking OD at 541 nm. The result clearly shows that the RBCs incubated with 800 $\mu g ml^{-1}$of the MoS_2-NSs, causes mild RBCs lysis. Therefore, our results demonstrated that MoS_2-NSs possessed haemocompatibility in lower concentration [39].

3.5 Behavioral analysis and clinical parameters for LD50 determination

Based on the results of lethal dose (LD50), further doses of MoS_2-NSs 0.5, 1.0 and 1.5 mg kg^{-1} were selected. No abnormal behavior or abnormal clinical signs were observed in doses of 0.5 and 1.0mg kg^{-1}, while 40% death and other clinical and behavioral changes such as loss of appetite, tremor, loss of body weight and passive behavior were observed in the group receiving 1.5 mg kg^{-1} of MoS_2-NSs.These changes occur due to effect of MoS_2 toxicity at LD50.

3.6 Body and Organ weights

The body weight of first two group mice wassimilaras compare to control groups, and no significant difference was observed, whereas, on the fourth day, group-III (1.5 mg kg^{-1}) mice shows significant increased body weight in comparison to control group (Figure 5a). Also, the different vital organs such as (liver, kidney and spleen) from MoS_2-NSs treated mice, showed no significant weight differences with control groups (Table 1).

3.7Hematological analysis

Major hematological markers such as red blood cell counts (RBCs), hemoglobin (Hb), white blood cells (WBCs), mean corpuscular hemoglobin concentration (MCHC), platelet count (PLT), mean corpuscular hemoglobin (MCH), mean corpuscular volume (MCV) and hematocrit (HCT) were evaluated. Here, significant increased levels of Hb and MCV were observed in group-II (1.0 mg kg^{-1}) mice as compared to control. Furthermore, a significant decrease was observed in PLT count of group-III (1.5 mg kg^{-1}) mice as compared to control (Table 2). These changes are observed due to interact of nanosheets with blood cells and causes various immunogenic response like inflammation and alteration of signaling pathways, which alters the

hematological markers[40,41]. Detailed mechanism has been discussed in the forthcoming subsection.

3.8Effects of MoS_2-NSs on serum biochemical parameters

The blood serum of MoS_2-NSs treated mice were analyzed for biochemical markers such as alanine aminotransferase (ALT), aspartate aminotransferase (AST) and Alkaline Phosphatase (ALP). The serum biochemical assays shown an increase in the alanine (ALT/GPT) activity for group-III (1.5 mgkg^{-1}) mice. However, the highest doses of 1.5 mg kg^{-1} have found statistically significant effect in the increasing activity of ALT/GPT as compared with the control groups (Figure 5 b). Further the analysis of aspartate aminotransferases (AST/GOT) have been found a dose dependent increment on exposure to MoS_2-NSs treated mice. However, the increase was less significant up to group II (1.0 mg kg^{-1}) mice and becomes highly significant in group III (1.5 mg kg^{-1}) mice as compare to control (Figure 5 c). Another enzyme, alkaline phosphatase (ALP), has shown an increased activity at highest concentration (1.5 mg kg^{-1}) of MoS_2-NSs treated mice compared with control groups (Figure 5 d).

The blood biochemical parameters were monitored to evaluate the function of liver, kidney and spleen after the administration of MoS_2-NSs. The level of ALT has been tested along with AST and ALP to evaluate the liver function. It is seen that, whenever, liver become dysfunctional, the level of these blood biochemical enzymes (ALT, AST and ALP) rises.

According to our findings, significant increased level of ALT, AST and ALP (Figure 5 b, c and d) in serum might be associated with leak out of these enzymes in blood circulation due to triggered MoS_2-NSs stress. Biologically, serum glutamic pyruvic transaminase (SGPT) is most suitable parameter for justification of liver injury than SGOT, because serum glutamic oxaloacetic transaminase (SGOT) is also found in kidney and heart muscles. Some previous

studies have also reported that, in the case of hepatocellular injuries, the transportation of ALT and AST is disturbed which leads to leakage of ALT and ALP in general blood circulation and increase its activity[42,43].

On the other hand, the level of ALP in serum are associated to the function of hepatocytes [6]. In present study, we observed an elevation in the level of serum ALP (Figure 5(b)) in MoS_2-NSs treated mice. For this elevation, we assume that MoS_2-NSs must have affected the liver and may trigger the synthesis of ALP due to biliary pressure.

3.9Antioxidant Enzyme Assay in Organs

Oxidative stress is considered as an important mechanism for the toxicity evaluation of nanomaterials. In this study, anti-oxidative indicators of the liver, kidney and spleen were evaluated. The results have been shown in Figure 5.The lipid peroxidation level, measured by the thiobarbituric acid reactive substances (TBARS) assay (Figure 5 e), shows a significant increment in the MoS_2-NSs treated groups-II (1.0 mg kg^{-1}) and group-III (1.5 mg kg^{-1}) as compared with the control group ($p < 0.05$). The superoxide dismutase activity (SOD) (Figure 5 g) and the catalase activity (CAT) have shown a significant decrease in group-III (1.5 $mgkg^{-1}$) as compared with control group (p □ 0.05) (Figure 5 h). Likewise, the activities of glutathione peroxidase (GPx) were decreases significantly in group-III (1.5 mg kg^{-1}) as compared to control group (p □ 0.05) (Figure 5 f).

Oxidative stress is also an important parameter that plays a vital role in causing *in vivo* toxicity .To evaluate, the role of oxidative stress due to MoS_2-NSs treatment, the level of Malondialdehyde (MDA) in the liver, kidney and spleen homogenates were assessed. The TBARS assay results revealed that the level of MDA increased significantly in the homogenates of liver, kidney and spleen of group-III (1.5 $mgkg^{-1}$) treated mice (Figure 5 e), while a significant

elevation in MDA level in liver homogenate only was reported in case of group-II (1.0 mg kg^{-1}) treated mice. The elevation in the level of MDA primarily suggests that increased lipid peroxidation during tissue damage, suppresses the activity of anti-oxidants which prevent excessive free radical formation. In general, liver is the main organ for detoxification of hazardous materials and chemicals, So there is the high risk for reactive oxygen species (free radical) attack, leading lipid peroxidation and causes hepatotoxicity [44].Numerous other studies also supports lipid peroxidation *via* free radical generation due to nanoparticles induced toxicity[45,46]. Our results are also in accordance with other report that MoS_2 increased lipid peroxidation in mice[47].

The result obtained from the present study clearly shows that the high dose (1.5 mg kg^{-1}) administered in group –III mice has significant reduction in the level of SOD, CAT and GPx activity (Figure 5f,g,h) due to excessive production of reactive oxygen species (ROS).Li *et al.* reported that SOD activity could be suppressed due to excessive superoxide radicals formation and H_2O_2 accumulation[48]. The toxicity due to the higher dose of MoS_2-NSs is mainly due to the generation of ROS. The detailed mechanism has been discussed in the forthcoming subsection.

Our results are also supported by other *in vivo* studies using different nanomaterials that possess the ability to elevate the oxidative stress. Similar to our findings, the experimental results using TiO_2 has been confirmed to increase the hepatic injuries and significant alteration in antioxidants level[49,50].

3.10Histopathological examinations

The histological sections of liver, kidney and spleen were observed. The morphological changes in the processed organs were examined. Figures 6 summarize the histological alteration in each group.

The microscopic observations of the control liver section, (Figure 6 a), showed normal structure and compact arrangement of hepatocytes. No obvious hepatic damage was observed in group-I and group-II in comparison to control group. However, significant morphological alteration like hepatocytes degeneration, mild necrosis, partial damage of central vein and hepatocyte vacuolation were observed in liver tissue (Figure 6 d) of group-III mice as compared to control group.

Histopathological study of kidney shows no remarkable alteration in group-I and group-II mice, as compared with the control group. However, group-III (1.5 mg kg^{-1}) mice (Figure 6h) show mild nephrotoxicity, such as swelling of glomerulus and decreased bowman's space.

In case of spleen histological sections, none of the MoS_2-NSs treated groups shows any significant pathological alteration, as compared with the control group (Figure 6 J,K,L).Further, histopathological evaluation was performed to observe any alteration in the morphology of the liver, kidney and spleen tissues. The histopathologies of liver of group-I (0.5 mg kg^{-1}) and group-II (1.0 mg kg^{-1}) (Figure 6 b, c) shows no morphological alteration in hepatocytes. However group-III (1.5 mg kg^{-1}) mice show hydropic degeneration, mild necrosis, partial damage of central vein and hepatocyte vacuolation (Figure 6 d).

Kupffer cells are local macrophages of liver and involve in defense of liver against hazardous chemical and materials. Activation of these cells by hazardous chemical and materials

induce to release inflammatory stuffs, growth modulators and ROS. Thus activation of Kupffer cells temper hepatic injury and chronic liver reactions[51]. Zhao *et. al*. reported that abdominal administration of nanoanatase TiO_2 in mice causes kidney toxicity due to excessive generation of ROS, which leads lipid peroxidation and failure of antioxidant defense mechanism[52].

Histopathological study of kidney shows no remarkable alteration in group-I (0.5 mg kg^{-1}) and group-II (1.0 mg kg^{-1}) (figure 6 f, g) mice, as compared with the control group. However, group-III (1.5 mg kg^{-1}) (Figure 6 h) mice show mild nephrotoxicity, swelling in renal glomeruli.

The results obtained from our study showed that high concentration of MoS2 nanosheets show abnormal signs. As an evidence, after autopsy we found that a large number of nanostructures are accumulated in intraperitoneal cavity of group-III (1.5 mg kg^{-1}) mice and some are adhere onto the organs such as liver, kidney and spleen. Some previous studies also supports our result that nanoparticles can easily cross the wall of small intestine by absorption and then transported into different body parts like brain, lung, heart, kidney, liver, spleen and stomach through circulatory system[53].

3.11Determination of apoptosis by Acridine orange–ethidium bromide (AO–EtBr) staining

The splenocytes cells isolated from the spleen of the MoS_2-NSs treated mice showed an increased apoptotic bodies (Figure 7) as examined by the AO–EtBr staining. The dead cells that showed red color are few in number and the cause of death might be apoptotic as well as necrotic, however, we obtain most of the cells are viable emitting green colordue to acridine orange dye uptake.

The result obtained from AO-EtBr staining, clearly suggest that ROS must change the membrane potential of the spleenocytes which is the major reason for apoptosis of spleenocytes as shown by the AO–EtBr staining[27].

3.12 Mechanism for MoS_2-NSs based toxicity

The mechanism of ROS generation by MoS_2-NSs is shown in figure 8. Interaction of MoS_2-NSs with Kupffer cell may activate it to produce inflammatory mediators, growth factors and reactive oxygen species (ROS)[51].Sulfur vacancies present at the edge of MoS_2-NSs acts as electron donor to catalyze oxygen molecules in to superoxide ions[54]. These superoxide ionsare the precursor for most of the ROS generation[55].

$$O_2 + MoS_2(e^-) \rightarrow {}^{*}O_2^- \quad (1)$$

$$H_2O_2 + e^- \rightarrow OH^- + {}^{*}OH \quad (2)$$

These generated ROS may cause antioxidant depletion, hepatic injuries and increases the lipid peroxidation[56–58].

4. Conclusion

In summary, we have synthesizedMoS_2-NSs by facile and eco-friendly hydrothermal method using sodium molybdate and L-Cysteine. Further *in vitro* and *in vivo* toxicity studies have been performed using different concentration of MoS_2-NSs. The *in vitro* study results suggest that at lower concentration MoS_2-NSs does not causes any toxicity. While, *in vivo* study results conclude that serum biochemical markers were hiked significantly at higher concentration of MoS_2-NSs (1.5 mg kg^{-1}). Also, higher concentration significantly decreased the antioxidant enzymes activity. Histopathological studies in response to higher dose of MoS_2-NSs treatment also shows altered architecture of liver as well as kidney, while spleen morphology remains

unaltered. The toxicity of MoS_2-NSs is supposed due to the ROS generation mainly. Due to significant importance of MoS_2-NSs, present study suggests that lower concentration can be permissible concentration for the biomedical applications; however, improving the dispersion in aqueous media and surface coating of MoS_2-NSs might further allow application of higher doses. Furthermore, other toxicological parameters are also needed to evaluate the harmful biological responses associated with MoS_2-NSs in future.

Acknowledgements

Authors are thankful to UGC New Delhi for financially supported, CAS Department of Zoology and Physics, BHU, Varanasi, India. Authors are also thankful to DST, New Delhi, India for financial support under DST-PURSE (Scheme-5050).

Conflict of Interests: Authors have no conflict of interests.

Funding Statement: Authors have no specific grant, from any funding agency for publication.

References:

[1] M. Chhowalla, Z. Liu, H. Zhang, Two-dimensional transition metal dichalcogenide (TMD) nanosheets, Chem. Soc. Rev. 44 (2015) 2584–2586. doi:10.1039/C5CS90037A.

[2] H. Tian, M.L. Chin, S. Najmaei, Q. Guo, F. Xia, H. Wang, M. Dubey, Optoelectronic devices based on two-dimensional transition metal dichalcogenides, Nano Res. 9 (2016) 1543–1560. doi:10.1007/s12274-016-1034-9.

[3] A. Molina-s, D. Sangalli, K. Hummer, A. Marini, L. Wirtz, Effect of spin-orbit interaction on the optical spectra of single-layer , double-layer , and bulk MoS 2, Phys. Rev. B. 88 (2013) 1–6. doi:10.1103/PhysRevB.88.045412.

[4] J. Yang, D. Voiry, S.J. Ahn, D. Kang, A.Y. Kim, M. Chhowalla, H.S. Shin, Two-Dimensional Hybrid Nanosheets of Tungsten Disulfide and Reduced Graphene Oxide as Catalysts for Enhanced Hydrogen Evolution, Angew. Chemie Int. Ed. 52 (2013) 13751–13754. doi:10.1002/anie.201307475.

[5] Q. Tang, Z. Zhou, Graphene-analogous low-dimensional materials, Prog. Mater. Sci. 58 (2013) 1244–1315. doi:https://doi.org/10.1016/j.pmatsci.2013.04.003.

[6] S.Z. Butler, S.M. Hollen, L. Cao, Y. Cui, J.A. Gupta, H.R. Gutierrez, T.F. Heinz, S.S. Hong, J. Huang, A.F. Ismach, E. Johnston-Halperin, M. Kuno, V. V Plashnitsa, R.D. Robinson, R.S. Ruoff, S. Salahuddin, J. Shan, L. Shi, M.G. Spencer, M. Terrones, W. Windl, J.E. Goldberger, Progress, challenges, and opportunities in two-dimensional materials beyond graphene., ACS Nano. 7 (2013) 2898–2926. doi:10.1021/nn400280c.

[7] E.L.K. Chng, M. Pumera, Toxicity of graphene related materials and transition metal dichalcogenides, RSC Adv. 5 (2015) 3074–3080. doi:10.1039/C4RA12624F.

[8] A.P. Nikalje, Nanotechnology and its Applications in Medicine, Med. Chem. (Los. Angeles). 5 (2015) 1–9. doi:10.4172/2161-0444.1000247.

[9] W. Yin, L. Yan, J. Yu, G. Tian, L. Zhou, X. Zheng, X. Zhang, High-Throughput Synthesis of Single- Layer MoS2 Nanosheets as a Near- Infrared Photothermal-Triggered Drug Delivery for E ff ective Cancer Therapy, ACS Nan. 8 (2014) 6922–6933. doi:10.1021/nn501647j.

[10] X. Liu, D. Ma, H. Tang, L. Tan, Q. Xie, Y. Zhang, M. Ma, S. Yao, Polyamidoamine Dendrimer and Oleic Acid-Functionalized Graphene as Biocompatible and Efficient Gene Delivery Vectors, ACS Appl. Mater. Interfaces. 6 (2014) 8173–8183. doi:10.1021/am500812h.

[11] Z. Kou, X. Wang, R. Yuan, H. Chen, Q. Zhi, L. Gao, B. Wang, Z. Guo, X. Xue, W. Cao, L. Guo, A promising gene delivery system developed from PEGylated MoS2 nanosheets for gene therapy., Nanoscale Res. Lett. 9 (2014) 587. doi:10.1186/1556-276X-9-587.

[12] M. Pumera, A.H. Loo, Layered transition-metal dichalcogenides (MoS2 and WS2) for sensing and biosensing, TrAC Trends Anal. Chem. 61 (2014) 49–53. doi:https://doi.org/10.1016/j.trac.2014.05.009.

[13] G. Lalwani, A.M. Henslee, B. Farshid, P. Parmar, L. Lin, Y.-X. Qin, F.K. Kasper, A.G. Mikos, B. Sitharaman, Tungsten disulfide nanotubes reinforced biodegradable polymers for bone tissue engineering, Acta Biomater. 9 (2013) 8365–8373. doi:https://doi.org/10.1016/j.actbio.2013.05.018.

[14] M. Balcioglu, M. Rana, N. Robertson, M. V Yigit, DNA-Length-Dependent Quenching of Fluorescently Labeled Iron Oxide Nanoparticles with Gold , Graphene Oxide and MoS 2

Nanostructures, ACS Appl. Mater. Interfaces. 6 (2014) 12100–12110.

[15] S. Wu, Z. Zeng, Q. He, Z. Wang, S.J. Wang, Y. Du, Z. Yin, X. Sun, W. Chen, H. Zhang, Electrochemically Reduced Single-Layer MoS 2 Nanosheets : Characterization , Properties , and Sensing Applications, Sensors. 8 (2012) 2264–2270. doi:10.1002/smll.201200044.

[16] B.L. Li, J. Wang, H.L. Zou, S. Garaj, C.T. Lim, J. Xie, N.B. Li, D.T. Leong, Low-Dimensional Transition Metal Dichalcogenide Nanostructures Based Sensors, Adv. Funct. Mater. 26 (2016) 7034–7056. doi:10.1002/adfm.201602136.

[17] H. Zhang, K.P. Loh, C.H. Sow, H. Gu, X. Su, C. Huang, Z.K. Chen, Surface modification studies of edge-oriented molybdenum sulfide nanosheets., Langmuir. 20 (2004) 6914–6920. doi:10.1021/la049887t.

[18] C. Zhu, Z. Zeng, H. Li, F. Li, C. Fan, H. Zhang, Single-Layer MoS2-Based Nanoprobes for Homogeneous Detection of Biomolecules, J. Am. Chem. Soc. 135 (2013) 5998–6001. doi:10.1021/ja4019572.

[19] N.C. Andres, N.L. D'Elia, J.M. Ruso, A.E. Campelo, V.L. Massheimer, P. V Messina, Manipulation of Mg(2+)-Ca(2+) Switch on the Development of Bone Mimetic Hydroxyapatite., ACS Appl. Mater. Interfaces. 9 (2017) 15698–15710. doi:10.1021/acsami.7b02241.

[20] R. Das, H. Mishra, A. Srivastava, A.M. Kayastha, Covalent immobilization of β-amylase onto functionalized molybdenum sulfide nanosheets, its kinetics and stability studies: A gateway to boost enzyme application, Chem. Eng. J. 328 (2017) 215–227. doi:https://doi.org/10.1016/j.cej.2017.07.019.

[21] S. Irwin, Comprehensive Observational Assessment□: Ia . A Systematic, Quantitative Procedure for Assessing the Behavioral and Physiologic State of the Mouse, Psychopharmacologia. 13 (1968) 222–257. doi:10.1007/bf00401402.

[22] M.M. Bradford, A rapid and sensitive method for the quantitation of microgram quantities of protein utilizing the principle of protein-dye binding., Anal. Biochem. 72 (1976) 248–54. http://www.ncbi.nlm.nih.gov/pubmed/942051 (accessed January 5, 2017).

[23] H. Ohkawa, N. Ohishi, K. Yagi, Reaction of linoleic acid hydroperoxide with thiobarbituric acid., J. Lipid Res. 19 (1978) 1053–7. http://www.ncbi.nlm.nih.gov/pubmed/103988 (accessed January 5, 2017).

[24] K. Das, L. Samanta, G.B.N. Chainy, A modified spectrophotometric assay of superoxide dismutase using nitrite formation by superoxide radicals, Indian J. Biochem. Biophys. 37 (2000) 201–204. http://www.renovacionterritorio.gov.co/librerias/media/pdf/ART_plan_estrategico.pdf.

[25] A.K. Sinha, Calorimetric Assay of Catalase, Anal. Biochem. 47 (1972) 389–394. doi:10.1016/0003-2697(72)90132-7.

[26] S. V Mantha, M. Prasad, J. Kalra, K. Prasad, Antioxidant enzymes in hypercholesterolemia and effects of vitamin E in rabbits, Atherosclerosis. 101 (1993) 135–144. doi:10.1016/0021-9150(93)90110-g.

[27] S. Goswami, C. Haldar, UVB irradiation severely induces systemic tissue injury by augmenting oxidative load in a tropical rodent: efficacy of melatonin as an antioxidant., J. Photochem. Photobiol. B. 141 (2014) 84–92. doi:10.1016/j.jphotobiol.2014.08.027.

[28] L. Yang, X. Cui, J. Zhang, K. Wang, M. Shen, S. Zeng, S.A. Dayeh, L. Feng, B. Xiang,

Lattice strain effects on the optical properties of MoS2 nanosheets, Sci. Rep. 4 (2014) 5649. doi:10.1038/srep05649.

[29] G. Deokar, D. Vignaud, R. Arenal, P. Louette, J.-F. Colomer, Synthesis and characterization of MoS2 nanosheets, Nanotechnology. 27 (2016) 75604. doi:10.1088/0957-4484/27/7/075604.

[30] H.D. Ha, D.J. Han, J.S. Choi, M. Park, T.S. Seo, Dual Role of Blue Luminescent MoS2 Quantum Dots in Fluorescence Resonance Energy Transfer Phenomenon, Small. 10 (2014) 3858–62. doi:10.1002/smll.201400988.

[31] W. Dai, H. Dong, B. Fugetsu, Y. Cao, H. Lu, X. Zhang, Tunable Fabrication of Molybdenum Disulfi de Quantum Dots for Intracellular MicroRNA Detection and Multiphoton Bioimaging, Small. 11 (2015) 4158–4164. doi:10.1002/smll.201500208.

[32] B. Farshid, G. Lalwani, B. Sitharaman, *In vitro* cytocompatibility of one-dimensional and two-dimensional nanostructure-reinforced biodegradable polymeric nanocomposites, J. Biomed. Mater. Res. Part A. 103 (2015) 2309–2321. doi:10.1002/jbm.a.35363.

[33] H. Wu, R. Yang, B. Song, Q. Han, J. Li, Y. Zhang, Y. Fang, R. Tenne, C. Wang, Biocompatible Inorganic Fullerene- Nanoparticles Produced by Pulsed Laser Ablation in Water, ACS Nano. 5 (2011) 1276–1281. doi:10.1021/nn102941b.

[34] E.L.K. Chng, Z. Sofer, M. Pumera, MoS2 exhibits stronger toxicity with increased exfoliation, Nanoscale. 6 (2014) 14412–14418. doi:10.1039/C4NR04907A.

[35] Y. Zhang, W. Xiu, Y. Sun, D. Zhu, Q. Zhang, L. Yuwen, L. Weng, Z. Teng, L. Wang, RGD-QD-MoS2 nanosheets for targeted fluorescent imaging and photothermal therapy of cancer, Nanoscale. 9 (2017) 15835–15845. doi:10.1039/C7NR05278B.

[36] U. Yadav, H. Mishra, V. Singh, S. Kashyap, A. Srivastava, S. Yadav, P.S. Saxena, Enhanced Osteogenesis by Molybdenum Disulfide Nanosheet Reinforced Hydroxyapatite Nanocomposite Scaffolds, ACS Biomater. Sci. Eng. 5 (2019) 4511–4521. doi:10.1021/acsbiomaterials.9b00227.

[37] Y. Chong, Y. Ma, H. Shen, X. Tu, X. Zhou, J. Xu, J. Dai, S. Fan, Z. Zhang, The in vitro and in vivo toxicity of graphene quantum dots, Biomaterials. 35 (2014) 5041–5048. doi:10.1016/j.biomaterials.2014.03.021.

[38] K. Wang, Z. Gao, G. Gao, Y. Wo, Y. Wang, G. Shen, D. Cui, Systematic safety evaluation on photoluminescent carbon dots, Nanoscale Res. Lett. 8 (2013) 122. doi:https://doi.org/10.1186/1556-276X-8-122.

[39] L. Chen, X. Zhou, W. Nie, W. Feng, Q. Zhang, W. Wang, Y. Zhang, Z. Chen, P. Huang, C. He, Marriage of Albumin-Gadolinium Complexes and MoS2 Nanoflakes as Cancer Theranostics for Dual-Modality Magnetic Resonance/Photoacoustic Imaging and Photothermal Therapy., ACS Appl. Mater. Interfaces. 9 (2017) 17786–17798. doi:10.1021/acsami.7b04488.

[40] S. Kim, J.E. Choi, J. Choi, K.-H. Chung, K. Park, J. Yi, D.-Y. Ryu, Oxidative stress-dependent toxicity of silver nanoparticles in human hepatoma cells., Toxicol. In Vitro. 23 (2009) 1076–1084. doi:10.1016/j.tiv.2009.06.001.

[41] S. Shin, M. Ye, H. Kim, H. Kang, The effects of nano-silver on the proliferation and cytokine expression by peripheral blood mononuclear cells, Int. Immunopharmacol. 7 (2007) 1813–1818. doi:10.1016/j.intimp.2007.08.025.

[42] T. Hong, N. Tripathy, H. Son, K. Ha, H. Jeong, Y. Hahn, A comprehensive in vitro and in

vivo study of ZnO nanoparticles toxicity, J. Mater. Chem. B. 1 (2013) 2985–2992. doi:10.1039/c3tb20251h.

[43] O.S. Adeyemi, I. Adewumi, Biochemical Evaluation of Silver Nanoparticles in Wistar Rats, Int. Sch. Res. Not. 2014 (2014) 196091. doi:10.1155/2014/196091.

[44] A. Patlolla, P. Tchounwou, Biochemical and histopathological evaluation of functionalized single-walled carbon nanotubes in Swiss – Webster mice, J. Appl. Toxicol. 31 (2011) 75–83. doi:10.1002/jat.1579.

[45] S. Li, R. Zhu, H. Zhu, M. Xue, X. Sun, S. Yao, S. Wang, Nanotoxicity of TiO2 nanoparticles to erythrocyte in vitro, Food Chem. Toxicol. 46 (2008) 3626–3631. doi:10.1016/j.fct.2008.09.012.

[46] E. Park, J. Yi, K. Chung, D. Ryu, J. Choi, K. Park, Oxidative stress and apoptosis induced by titanium dioxide nanoparticles in cultured BEAS-2B cells, Toxicol. Lett. 180 (2008) 222–229. doi:10.1016/j.toxlet.2008.06.869.

[47] B. Fowler, M. Nordberg, B. Print, Handbook on the Toxicology of Metals, 2014.

[48] Z. Li, P. Li, T. Randak, Effect of a human pharmaceutical carbamazepine on antioxidant responses in brain of a model teleost in vitro : an efficient approach to biomonitoring, J. Appl. Toxicol. 30 (2010) 644–648. doi:10.1002/jat.1534.

[49] L. Ma, J. Liu, N. Li, J. Wang, Y. Duan, J. Yan, H. Liu, H. Wang, F. Hong, Oxidative stress in the brain of mice caused by translocated nanoparticulate TiO 2 delivered to the abdominal cavity, Biomaterials. 31 (2010) 99–105. doi:10.1016/j.biomaterials.2009.09.028.

[50] H. Liu, L. Ma, J. Liu, J. Zhao, J. Yan, F. Hong, Toxicological & Environmental Chemistry

Toxicity of nano-anatase TiO 2 to mice□: Liver injury , oxidative stress, Toxicol. Environ. Chem. 92 (2010) 175–186. doi:10.1080/02772240902732530.

[51] R.A. Roberts, P.E. Ganey, C. Ju, L.M. Kamendulis, I. Rusyn, J.E. Klaunig, Role of the Kupffer Cell in Mediating Hepatic Toxicity and Carcinogenesis, Toxicol. Sci. 96 (2007) 2–15. doi:10.1093/toxsci/kfl173.

[52] J. Zhao, N. Li, S. Wang, X. Zhao, J. Wang, J. Yan, J. Ruan, H. Wang, F. Hong, The mechanism of oxidative damage in the nephrotoxicity of mice caused by nano-anatase TiO2, J. Exp. Nanosci. 5 (2010) 447–462. doi:10.1080/17458081003628931.

[53] N.F. Hillyer, R.M. Albrecht, Gastrointestinal Persorption and Tissue Distribution of Differently Sized Colloidal Gold Nanoparticles, J. Pharm. Sci. 90 (2001) 1927–1936. doi:10.1002/jps.1143.

[54] S.V.P. Vattikuti, C. Byon, C.V. Reddy, R.V.S.S.N. Ravikumar, Improved photocatalytic activity of MoS2 nanosheets decorated with SnO2 nanoparticles, RSC Adv. 5 (2015) 86675–86684. doi:10.1039/c5ra15159g.

[55] J.F. Turrens, Mitochondrial formation of reactive oxygen species, J. Physiol. 552 (2003) 335–344. doi:10.1113/jphysiol.2003.049478.

[56] H. Wang, B. Zhou, S. Zhang, H. Guo, J. Zhang, J. Zhao, E. Tian, Reproductive toxicity in male mice after exposure to high molybdenum and low copper concentrations, Toxicol. Ind. Health. 32 (2016) 1598–1606. doi:10.1177/0748233715569269.

[57] T. Xia, M. Kovochich, M. Liong, L. Mädler, B. Gilbert, J.I. Yeh, J.I. Zink, A.E. Nel, Comparison of the Mechanism of Toxicity of Zinc Oxide and Cerium Oxide Nanoparticles Based on Dissolution and Oxidative Stress Properties, ACS Nano. 2 (2008)

2121–2134. doi:10.1021/nn800511k.

[58] A. Nel, T. Xia, L. Mädler, N. Li, Toxic Potential of Materials at the Nanolevel, Science (80-.). 311 (2006) 622–627. doi:10.1126/science.1114397.

Evaluation of *in vitro* and *in vivo* toxicity of pristine molybdenum disulphide nanosheets in Swiss albino mice

Umakant Yadav [a], *Vimal Singh* [a], *Himanshu Mishra* [b], *Preeti S. Saxena* [a*], *Anchal Srivastava* [b*]

[a]Department of Zoology, Institute of Science, Banaras Hindu University, Varanasi-221005, India.

[b]Department of Physics, Institute of Science, Banaras Hindu University, Varanasi-221005, India.

[*]**Corresponding authors**

Email: pssaxena@rediffmail.com (Dr. Preeti S. Saxena)

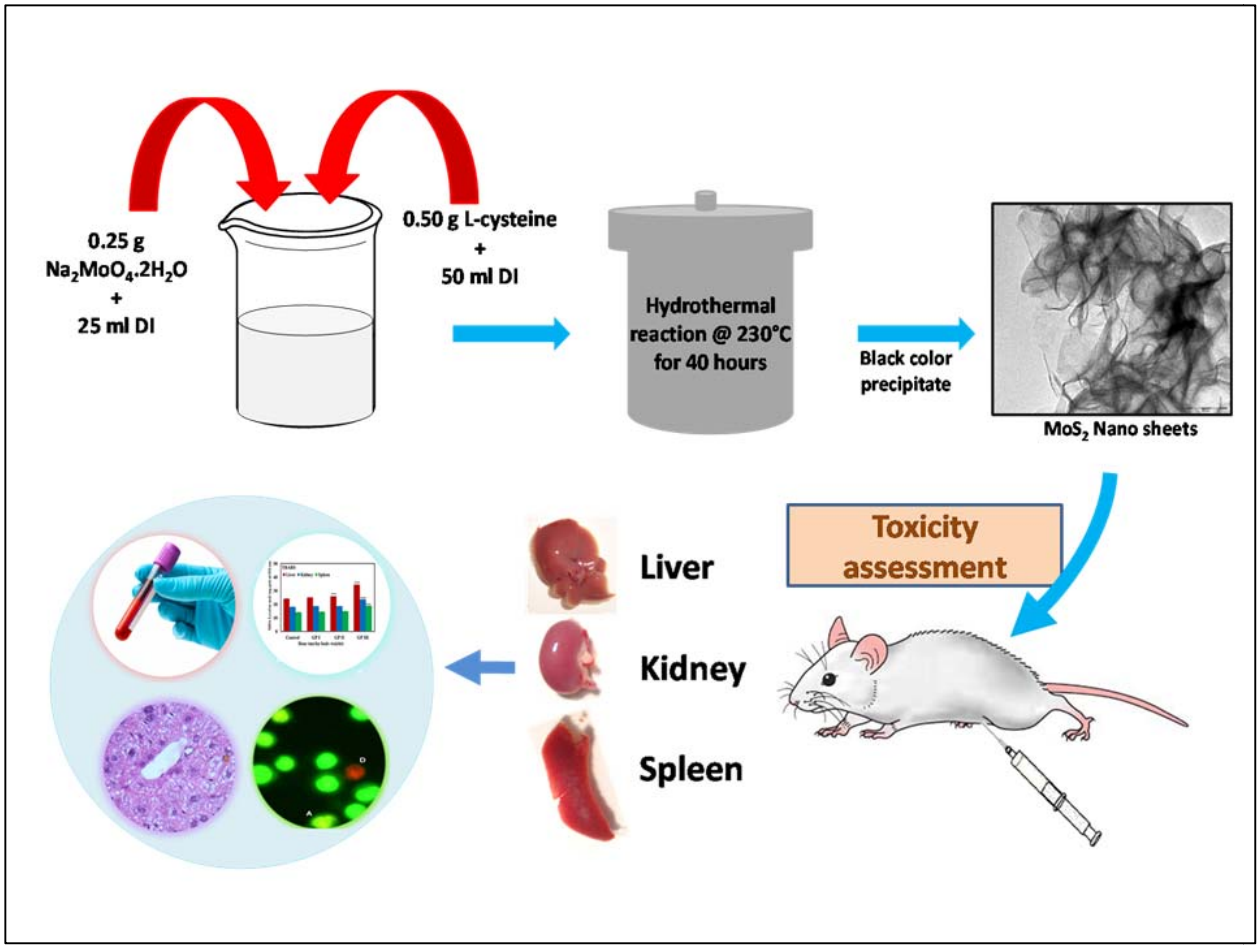

Figure 1: Schematic representation of for the synthesis and toxicity evaluation of MoS2-NSs.

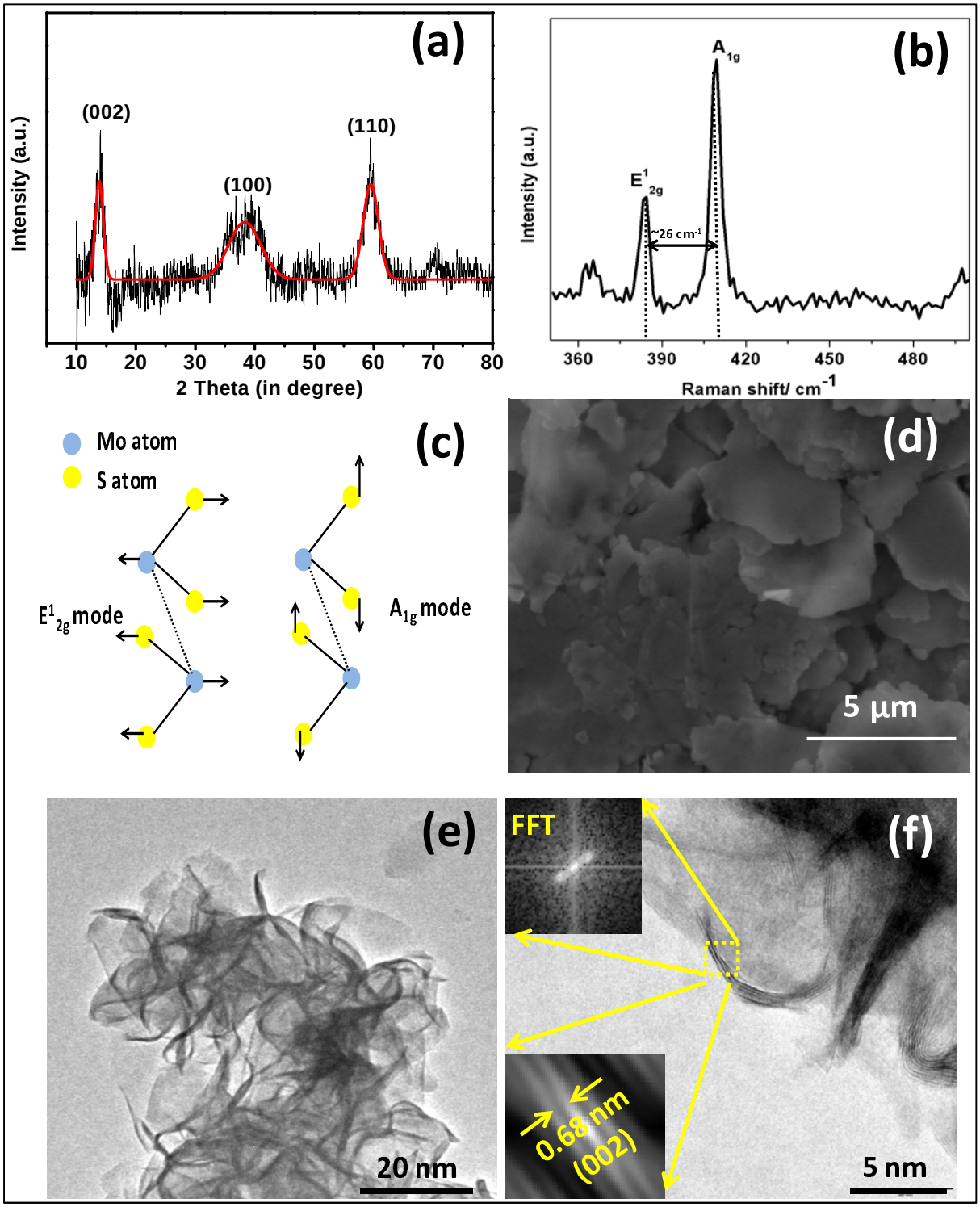

Figure 2: (a) XRD pattern, (b) Raman spectrum, (c) schematic for in-plane and out of plane vibrations, (d) SEM micrograph, (e) TEM micrograph, (f) HRTEM micrograph of multilayered MoS_2-NSs; Inset shows the FFT pattern and interlayer separation of multilayered MoS_2-NSs.

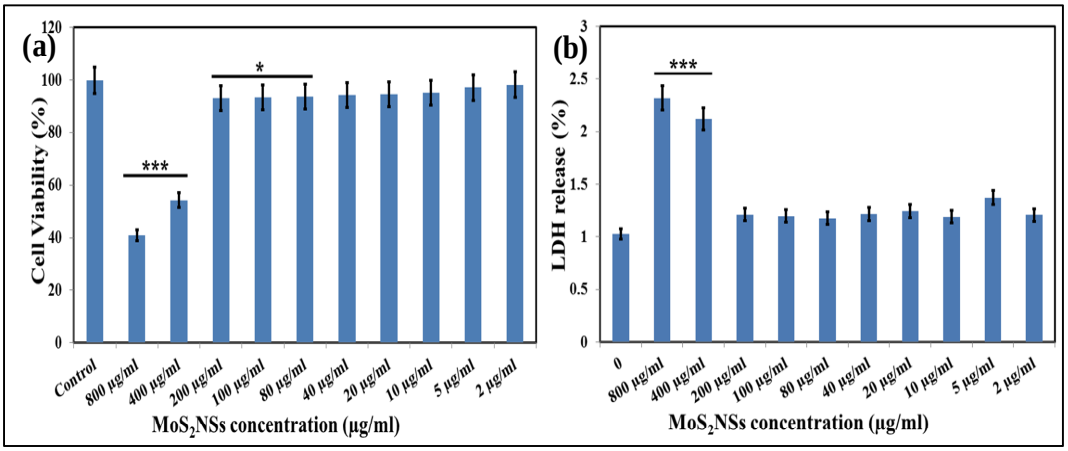

Figure 3: In vitro cytotoxicity tests: (a) MTT assay of MG-63 cells and (b) lactate dehydrogenase (LDH) release assay. Values are expressed as mean ± standard deviation (*P< 0.05,**P< 0.01,***P< 0.001, n= 3).

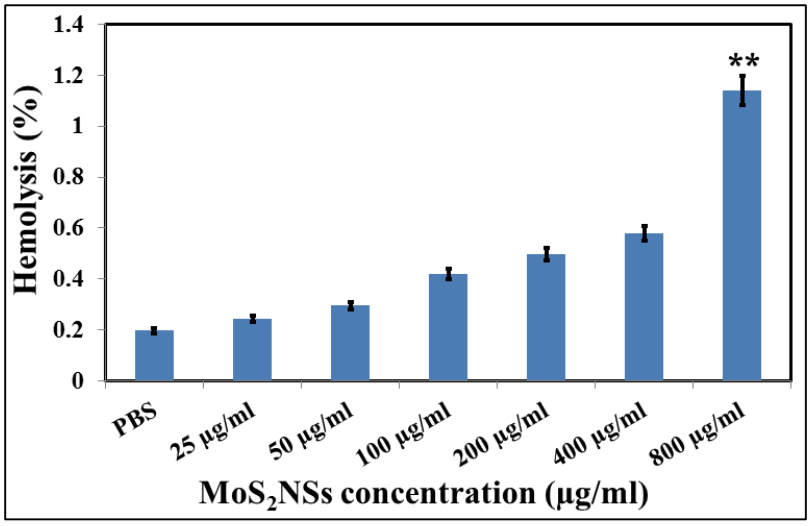

Figure 4: Shows the percentage hemolytic behavior of MoS_2-NSs.

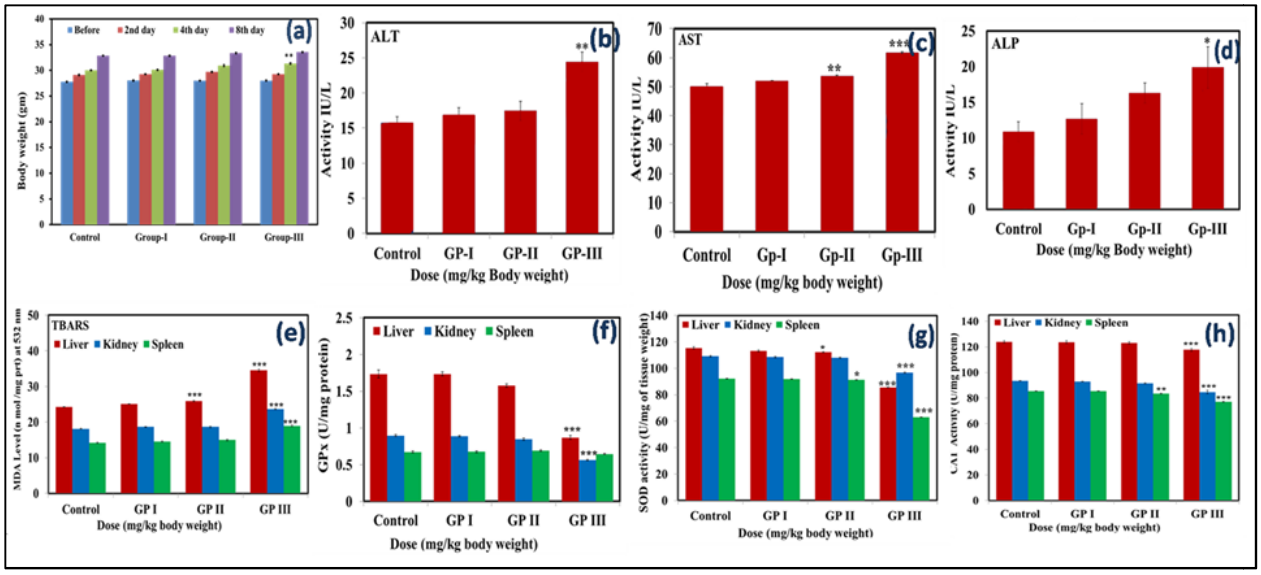

Figure 5: (**a**) Body weight of Control and MoS_2-NSs treated mice. (**b**) Bar diagram shows the activity of Alanine aminotransferase (ALT/GPT). **(c)** Aspartate aminotransferase (AST/GOT) and **(d)** Alkaline phosphatases (ALP) in the serum of control and treated groups mice. Each experiment was done in triplicate. **(e)** Shows the level of TBARS in the homogenate of liver, kidney and spleen of treated groups and control. (**f)** the activity of SOD (**g)**shows the activity of catalase and (**h)** the activity of Glutathione Peroxidase. Each experiment was performed in triplicate. Data represents mean ±SEM; n=5 mice. At *P<0.05 statistically significant when compared to control.

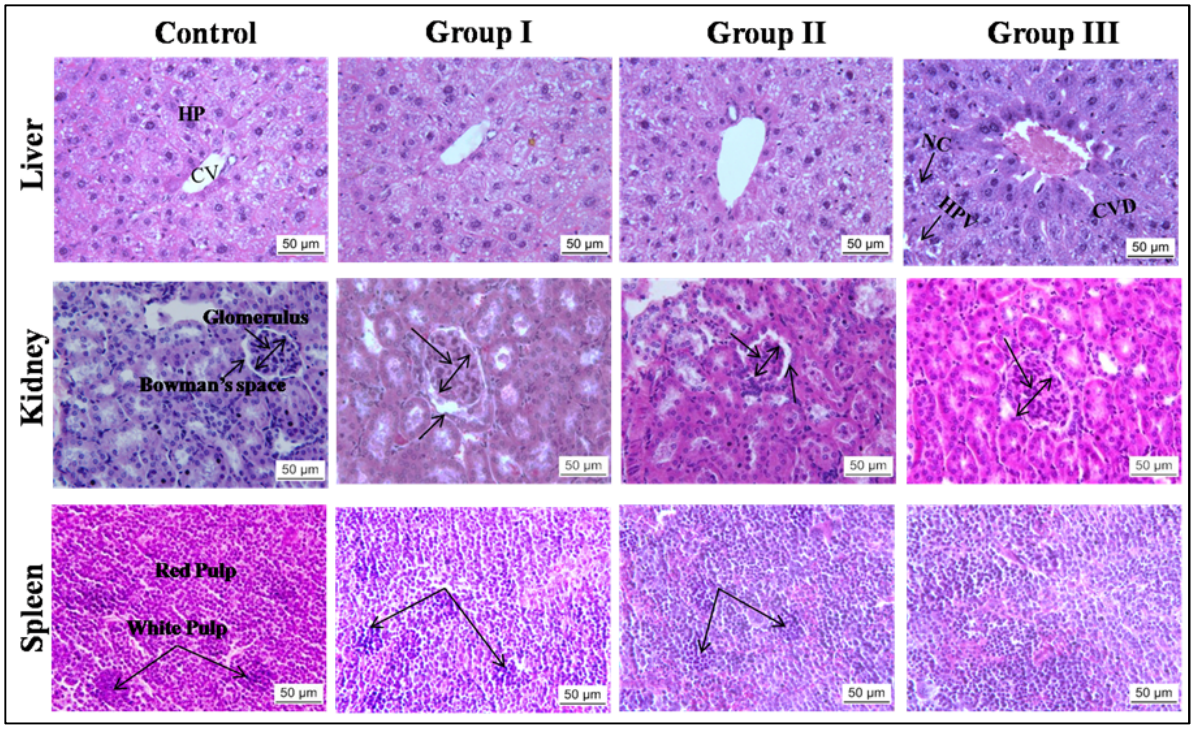

Figure 6: Histopathological evaluation (H&E staining, 40X) of organs in Swiss albino mice exposed to MoS_2-NSs. (A,E,I) Control group; (B,F,J) Group I- 0.5mgkg^{-1}; (C,G,K) Group II- 1.0 mgkg^{-1}; (D,H,L) = 1.5 mg kg^{-1}. (CV = central vein, HP= Hepatocytes, CVD= central vein damage, HPV = hepatocellular vacuolation NC = necrosis Glomerulus, Bowman's space, white Pulp and Red Pulp).

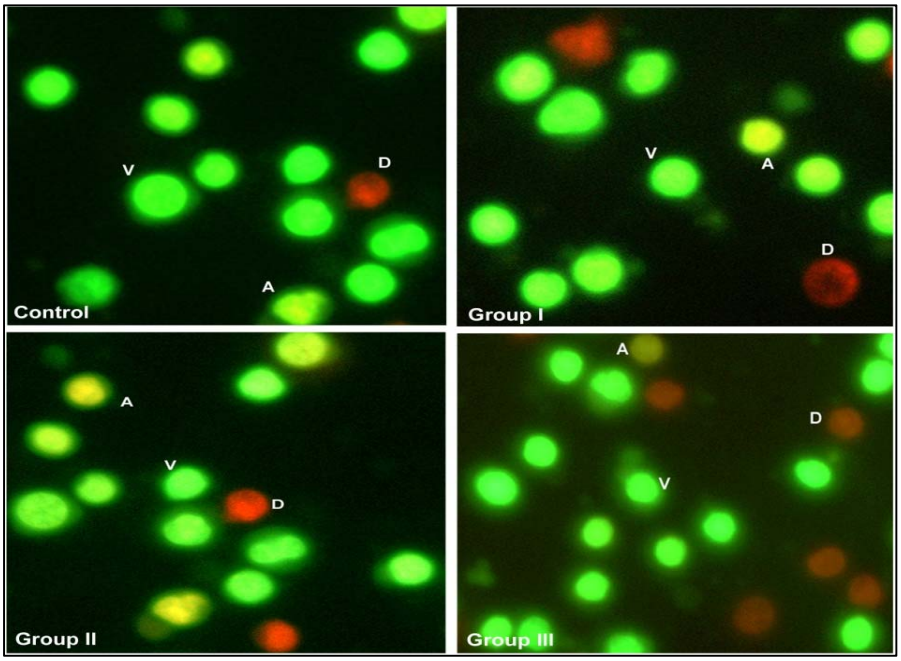

Figure 7: Staining of splenocytes with Acridine orange–ethidium bromide (AO–EtBr) showing apoptosis following the MoS_2-NSs administration. Apoptotic cells (orange) are denoted by the letter ‘‘A’’ while the green are normal viable cells denoted by ‘‘V’’. The red represents dead cells denoted by the letter ‘‘D’’.

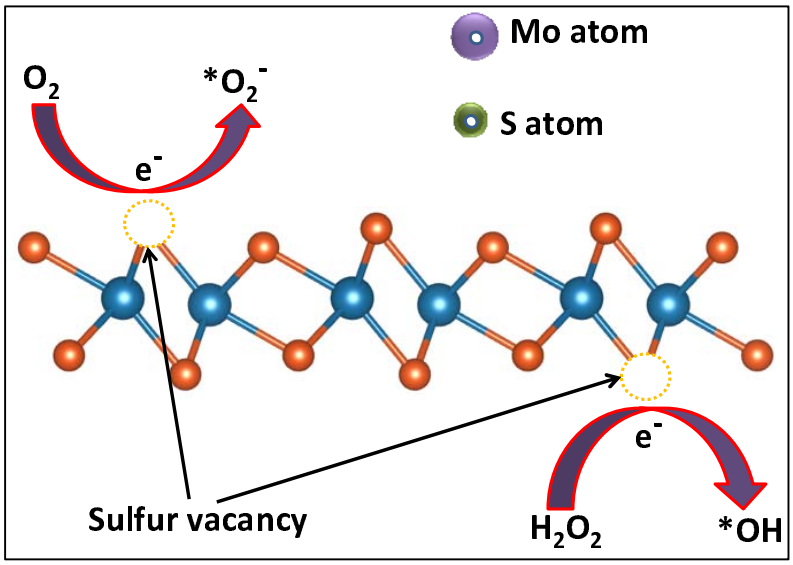

Figure 8: Schematic showing the mechanism of ROS generation due to MoS_2-NSs.